ACS OMEGA

Open Access

http://pubs.acs.org/journal/acsodf

Article

Revisiting Water Adsorption on TiO_2 and ZnO Surfaces: An SCC-DFTB Molecular Dynamics Study

Yarkın A. Çetin,* Laura Escorihuela, Benjamí Martorell, and Francesc Serratosa

Cite This: *ACS Omega* 2025, 10, 4449−4457

Read Online

ACCESS | Metrics & More | Article Recommendations | Supporting Information

ABSTRACT: Metal oxides (MOs) are the key materials in applications of biomedicine industrial technologies due to their versatile features. Knowing their possible toxicity level is crucial given some specific environments, particularly in water. We have learned that their reactivity almost depends on the electronic structure on the surface of the MOs. Thus, a detailed understanding of the electronic structure on the surface and its reactivity processes is useful for determining the toxicity in MOs and defining good descriptive parameters. We simulated the interaction of ZnO and TiO_2 slab models with water and checked their geometric and electronic structure changes from the bulk of the material to the water interface. To this end, we used the density functional tight binding theory coupled with finite temperature molecular dynamics. We have observed the interaction of water with the MO surface in terms of electronic and geometric parameters for several conditions, such as temperature, hydrogenated or clean, and exposed surface. In doing so, we provide molecular-level insights into topographical and electronic processes on MO surfaces besides finding critical points on the surface that can explain the initialization of dissolution processes. Thus, we reveal information about potential toxicity descriptors in a systematic analysis approach.

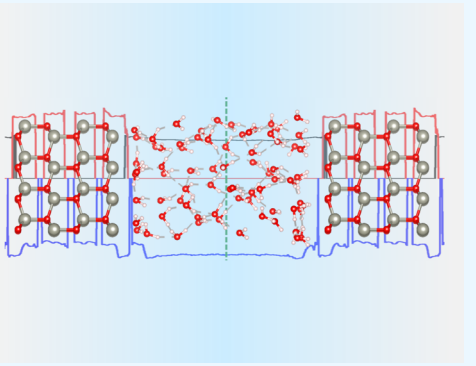

1. INTRODUCTION

Currently, there are a lot of common applications that use nanomaterials (NMs, particles that are smaller than 100 nm), and the tendency has kept growing during the last few years. These applications range from pesticides in the agricultural field[1] to nanobased personalized medicine,[2] the design of nanodevices based on nanoengineering,[3] the use as food coloring[4] or antibacterial implementation.[5]

The toxicity of NMs drastically differs from that of their corresponding bulk material. Moreover, its toxicity is highly dependent on the size distribution and dimension of the NMs.[6] Due to the growing demand for NMs, it is critical to study their toxicity in all different applications and possible parameter configurations. The physicochemical properties of materials are closely related to material toxicity. In the case of NMs, the unique characterization of physicochemical properties is a challenging task due to the variability of these properties with size, dimensions, and working conditions. Moreover, it is also crucial to know the nanoparticle material behavior in water since the interaction of the NMs surface with water may change the physicochemical properties of the material and the interaction in vivo conditions.[7−9]

On the industrial scale, titanium dioxide (TiO_2) is one of the most important nanocompounds since it is in use in many applications.[10,11] Another similar example could be zinc oxide (ZnO). Nevertheless, some studies suggest that ZnO and TiO_2 could penetrate human skin, thus being potentially hazardous to human health.[12−14] TiO_2 and ZnO NMs are known as examples of toxic metal oxides NMs with their ion-shedding ability.[15−17] Accordingly, deducing the knowledge underlying the physicochemical process of NMs is essential for describing their toxicology. For instance, one important chemical connection to describe their cytotoxicity is the prediction of forming Reactive Oxygen Species (ROS), which. Relates directly to the material's bandgap value (i.e., conduction and valence band energy difference, a well-studied physicochemical property).[18−27]

As much as electronic structure properties, the structural and geometry (size, stoichiometry, exposed surface, and defects···) features of NMs are another determinant factor in nanotoxicology.[28] As a particular example, the ZnO surface area is in correlation with toxicity.[29] For example, ZnO, smaller NMs could generate more ROS than larger particles (100−1000 nm) due to the larger ratio of exposed surface area and the increased ability to absorb UV light for photochemical reactions and the creation of highly reactive ROS.[23,30]

This study focuses on specific Metal Oxides (MO). We explore frequently exposed, stable Wurzite ZnO (001) and

Received: August 15, 2024
Revised: December 26, 2024
Accepted: January 3, 2025
Published: February 2, 2025

Anatase TiO_2 (101) surface behaviors and water interactions. Nevertheless, the mechanism of interaction between water-MO and water−water molecules is a dynamic system at room temperature that affects the electronic and geometry structures of the interface and possibly the toxicity of the NMs. The dynamic interaction of water with MO surfaces not only influences the redistribution of electronic charge but also affects ROS formation processes, which are directly linked to the cytotoxicity and genotoxicity of these materials in aquatic environments. While periodic boundary conditions simulate infinite slabs, these surfaces represent commonly exposed facets of ZnO and TiO_2 nanoparticles, making the results relevant for understanding NM-water interactions.[31,32]

In order to complement the present studies in the MO-water interface description, we decided to study at quasi-electronic structure methods the dynamic behavior of water on MO surfaces, without the present restrictions of density functional theory (DFT) that localize the study for static calculations of single or small clusters of water, or at most using one or two water adsorption layers on the surface at the DFT level. For instance, in recent studies, Zeng et al. explored the adsorption and reaction splitting of water on the TiO_2 surface but limited the molecular dynamics (MD) simulation to only two water adsorption layers for 2.0 ps,[33,34] or Li et al. performed the MD exploration of adsorbed single water molecules on TiO_2 for 4.0 ps.

Density Functional Tight Binding (DFTB) is a computationally efficient alternative to DFT that has shown consistent results with DFT in electronic structure calculations, including bandgap predictions. In some cases, DFTB has provided more accurate electronic interactions in periodic boundary conditions (PBC) calculations due to its parametrization approach using Hybrid functional calculations at the DFT level.[35,36] Therefore, using MD simulations at the DFTB level, we were able to go a step further. We analyzed the interaction of water with the MO through the redistribution of the geometry and electronic charge on the MO and the water interface. With such a method, no limitations on electronic structure redistribution or chemistry are imposed, as in the case of classic or reactive force field MD simulations.

2. RESULTS

In this section, we report results referring to our electronic and geometric analyses of the studied systems after MD simulations. Figures 1 and 2 represent the oxygen atom population and the electron charge distribution on species, respectively, for water interacting with slabs of ZnO and TiO_2 at different temperatures and surface hydrogenation conditions. Because of PBC, we visualized two unit cells on plots. The topography of the O atoms in Figure 1 allows the location of the slab layers as well as distinguishing water adsorbed on the interface and free bulk water in the simulations. On the other hand, Figure 2 represents the net charge on elements in identically overlapping unit areas of Figure 1.

Figures 1 and 2 follow the same scheme of 6 insets distributed in 3 rows and 2 columns. Each column is dedicated to one base material, i.e., ZnO or TiO_2, respectively. The top row shows results for bare MO-water systems at 300 K; the middle row is for bare MO-water systems at 600 K; the bottom row shows results when the surface is fully hydrogenated at 300 K. Consequently, each row represents the MO-water interface for different chemical conditions: first row at mild, room temperature conditions; middle row at very aggressive high temperature and pressure conditions; and bottom row at room temperature, at a hydrogen-terminated surface. This less stable slab model with a hydrogenated surface may resemble low pH conditions with an H^+ saturated solution; however, in our models, we do not take into account charges on the surface or negative counterions, which would be required for better modeling in low pH conditions, due to the limitations in computational capacities of the methodology.

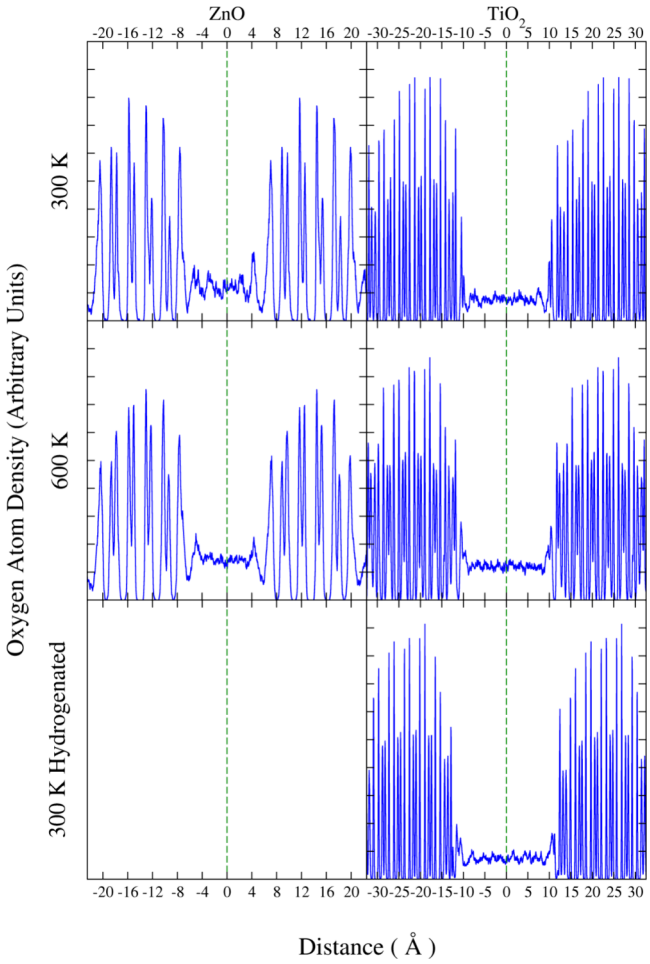

Figure 1. Oxygen atom population of the MO-water simulation systems at 300 K, 600 K and hydrogenated 300 K. Distance of the O atoms with respect to the center of the water bulk.

Figure 2 displays computed charges for Zn, Ti, O, and H. In fully ionic systems, expected charges are +2, +4, −2, and +1. However, Figure 2 shows values near +0.55, +0.95, −0.5 to −0.7, and 0.35 e^- for these species, indicating significant covalency in bonding, together with an underestimation of absolute formal charges by DFTB. For further clarity, an example of a single-point calculation is provided in Figure S1 in the Supporting Information.

2.1. Analysis of Interactions of MO Surface with Water at 300 K. In Figure 1, insets depict the geometry profile of the desired of each molecular system. Since all our MD simulated structures were constructed with oxygen atoms, counting the oxygen atom population permits the numerical representation of structure topography. Figure 2 involves the same visual structure of atomic charge for each atomic species through the system. In both approaches, Figures 1 and 2 plot show the separate layers of crystal in the slab, two interaction

https://doi.org/10.1021/acsomega.4c07557
ACS Omega 2025, 10, 4449−4457

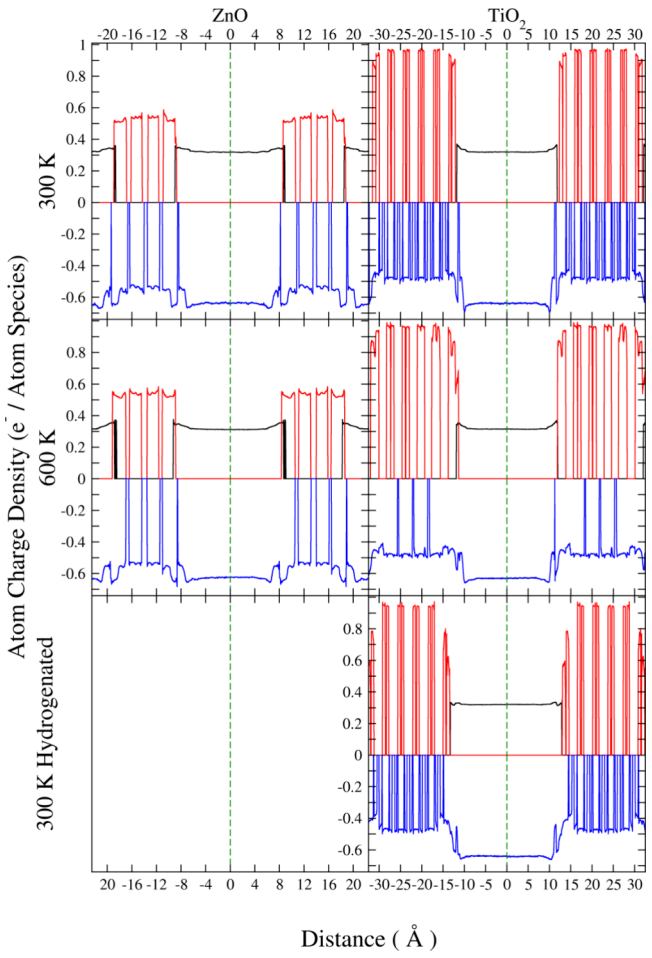

Figure 2. Formal charge of elements on the MO-water simulation systems at 300 K; 600 K and hydrogenated 300 K. Red for metal, blue for oxygen, black for hydrogen. Distance of atoms with respect to the center of the water bulk.

domains on the top and bottom sites of water-MO regions (interfaces of MO-water), and bulk solvent (H_2O) molecules.

Figure 1 inset 1.1 shows the oxygen atom distribution in the ZnO-water system at 300 K. The zinc oxide for this calculation was made of four layers of ZnO, which are easily observed in the figure, corresponding to the four double peaks between −20 and −8 Å, as well as the reproduction of the unit cell (in red) in the four double peaks between 8 and 20 Å. The peak at −8.3 Å corresponds to the Zn-terminated (001) surface, whereas the peak at 8.5 Å corresponds to the O-terminated surface (001). The distance between the two internal ZnO layers in the slab is 2.59 Å, close to the bulk distance of 2.60 Å. Around −7.8 Å appears a monolithic peak corresponding to H_2O molecules forming a first solvation layer on the surface, indicating a strong interaction of the Zn-terminated (001) phase and the aqueous phase. This peak is reproduced on the O-terminated face at 7.5 Å, as a first solvation shell; at 4.2 Å, it is observed as a second weaker solvation layer. Those peaks indicate that first solvation shells are occurring as frozen-like stationary layers with a retention time on the surface far beyond the simulation time in this work. The rest of the region between −7 and 4 Å corresponds to liquid water molecules. The average distances between the first solvation layer and ZnO layers are 1.99 and 2.28 Å, for Zn-terminated and O-terminated surfaces, respectively. These values are in accordance with DFT static[37,38] calculations and MD simulations,[39] in the range of 1.97−2.20 Å, being the interaction between Zn and O of the water molecule more stable; explaining why the O-terminated surface shows a longer distance.

The same analysis for TiO_2-water is in inset 1.2 of Figure 1. The TiO_2 model consists of six layers with symmetric terminations. These layers coincide on the tetra-furcate peaks between −30 and −12 Å (centered at −30.5, −27.1, −23.55, −20.05, −16.35, and −12.8 Å, respectively), which reproduces due to the periodicity between the 13.4 and 31 Å (at 13.4, 16.59, 20.3, 23.8, 27.45, and 31.15 Å) Peaks at −10 and 10 Å are the interacting frozen-like water molecules of the first solvation shell on the surface. A weak second shell is at −7.5 and 7.5 Å. The distance between the first solvation layer and TiO_2 is 2.01 Å with respect to the outermost Ti atoms. Ti−O bonds in the literature range from 2.10 to 2.25 Å.[40,41] This difference probably arises from the Ti plane definition in our model since Ti atoms are not perfectly on a straight plane but are corrugated.

Figures 1 and 2 are replicas of the same frame of the analysis approach. Therefore, the two sets of figures are superimposable. Figure 2 inset 1.1 displays the electron charge distribution on the whole ZnO-water system. We observe Zn (red) and H (black) charges in the positive ordinates, which are mutually excluded since water does not enter the MO region. On the negative side, O (blue) from the MO and water molecules are present. As a mirror of Figure 1 inset 1,1, the O atom charge accumulates in a pattern of four successive bars (in blue), indicating O atoms localization (ZnO layers) in the slab, and due to the structure organization of the MO, on this positive side, bars in red correspond to the Zn atoms' charge. Black ones represent the H atoms, associated with water molecules, between −8 and 8 Å. In the range of −8 to −4 Å in Figure 2 inset (1,1), we observe a solid surface influence on water molecules. In parallel, black and blue lines slightly change the slope. With respect to the higher slope from −8 to −6 Å (at −7 Å charge is 0.33 e^-), black lines become a plateau between −6 and −4 (at −5 Å charge is 0.32 e^-). Between −4 and 4 Å (along the interval, the charge is 0.31e^-), the line indicates that molecules behave as bulk water. Also, on the other face, the interaction zone reproduces itself with slightly different characteristics in the range 8−4 Å (charge at 7 and 5 Å is 0.33 e^- and 0.32 e^-).

In Figure 2 inset (1,1), at −10.2 Å, Zn atoms become less positive and O atoms become more negative on the first ZnO layer. Redline initiates 0.59 e^- (a typical value for DFTB oxides value in ZnO),[39] at 10.7 Å, and drops after −10.2 Å to 0.50 e^- (between −10.2 and −8.9 Å). Correspondingly, the population of the O atoms (blue line) takes −0.56 e^- at 10.7 Å, −0.67 e^- at −10.2 Å, and −0.66 e^- at −8.9 Å. This drop in 0.1 e^- is in the same line as found for single water molecules on ZnO for DFT calculations, indicating a charge transfer in the system.[39,42] As a consequence, on water molecules at −7.2 Å, the charge on the O atoms increases from −0.56 e^- (at −8.2 Å) to −0.68 e^- (−7.0 Å).

Figure 2, inset (1,2), covers the complete inspection components of TiO_2-water at 300 K. The MO-water interaction zone is observed in the H atoms line (in black), from −11.6 to −10.1 Å (charge is 0.36 e^-) and until −7.6 Å (charge is 0.32 e^-). In a reciprocal sense, between −13.5 and −11.8 Å, Ti atoms (red line) on the surface lose their positive electronic value in two intermediary step sections. Ti is 0.93 e^-

https://doi.org/10.1021/acsomega.4c07557
ACS Omega 2025, 10, 4449−4457

at −13.5 Å, and it drops 0.85 at −12.6 Å, and 0.89 e^- at −11.8 Å. This drop is less than 0.1 e^-, and DFT studies show a change from Ti^{4+} to Ti^{3+} is dictated by a charge transfer of 0.4 e;[43] therefore, Ti atoms are influenced by the presence of water molecules in the top layer, although not enough for a formal reduction of Ti atom. Charge of the O atom population at −13.5 Å (TiO_2 outer slab layer) is −0.50 e^-, and at −12.6 Å, subtends to −0.46 e^-, in good agreement with the reduction of water molecules at DFT calculations on TiO_2 (from −0.56 to −0.47 e^-).[34]

In general, for all shown cases, a reduction of the formal charges on atoms of the MO crystal and an increase of water molecule charges are observed. This interactive relation is evident in Figures 1 and 2 (e.g., in insets 1,2 of Figure 2, from −12.6 to −7.6 Å). In the −13.5 to −7.6 Å range, where the interaction is clearly observed, the absolute charge change from the two directions to the midpoint is 0.20 e^- on both sides. At that point, charge pack-like compartments are noticeable.

As a final remark in this section, water interacts strongly with the MO surface, and the first layers of water bulk sides gain a "frozen" like behavior. In ZnO there exists a polarization of water molecules on surfaces for Zn-terminated (−7.65 Å) or O-terminated (7.1 Å) slab layers. Surface charge reduction on metal atoms leads to a reciprocal increase in the charge of interacting first solvation layer water molecules. That ends up with a greater polarization of water molecules of the first layer on the surface. In the TiO_2 model, both sides of the slabs are O terminated and that polarization is less present due to the symmetry of the slab.

2.2. Analysis of the Interaction at Reactivity Conditions. *2.2.1. Analysis of the Interaction of the MO Surface with Water at 600 K.* In order to explore chemical reactions on the surface in the short time framework of our simulations, the temperature was increased up to 600 K; therefore, this section aims to explore the effect of temperature on the structure of water on MO crystals that are changed by temperature. This temperature was chosen because is typical in water-shift reactions on ZnO.[38,44] To be able to make direct comparisons with the systems at 300 K, the unit cell and water molecules were kept identical.

The effects of the temperature rise in the water simulations over MO are shown in the two middle insets of Figures 1 and 2 when compared with the corresponding above insets. In general trend, the mobilization of system components increased, particularly in bulk water and the solvation layers on the interfaces. When comparing inset 1.1 to inset 2.1 in Figure 1 (for ZnO), O atom peaks become symmetric on both terminations of the slab (between −8 and 8 Å). This phenomenon arises from less stable "frozen" water layers adsorbed on the interface. Peaks corresponding to the solid ZnO slab are barely affected by the rise of temperature in Figure 1. The liquid phase of the system (roughly through 6 Å to each side of the reference line) improves its plateau form by increasing temperature.

In the case of TiO_2−water (Figure 1 inset 1,2 at 300 K, and inset 2,2 at 600 K), the increased mobility in the system is reflected in the TiO_2 itself, with broader peaks in the slab (between −32 and −12.5 Å), indicating a greater excitation in the phonons. Peaks at 10 Å far from the reference line on the positive and negative sides get broadened, indicating a major mobility of water molecules in the first solvation layer. The rest of the bulk water shows similar behavior in both cases in those simulations for the O-counting distribution.

In Figure 2 (inset 2,1), the ZnO-water interaction is recognized between −8 and −4 Å, and at 8 to 4 Å. The 9 Å tick reflects the H atoms' position kept around surfaces and depolarization of charge, which coincides with the escalating H charge line form in black. Furthermore, related to this charge delocalization, we observe more negatively charged oxygens and more positively charged zinc atoms.

The same representative organization was followed on the TiO_2 crystal in Figure 2 (inset 2,2), with six layers of the solid phase between −31.95 and −11.25 Å and also on the positive side by system periodicity. Toward −15 to −11.1 Å (and as a mirror in the positive site), charge delocalization is visible between the three basis atom types in the system. The overall increase of mobilization in the system due to temperature decreases the vertical lines in solid phase representation. In parallel, water molecules' H atoms may be found englobed in the first, water-facing metal layers. This fact points to highly mobilized individual molecules and reciprocal crystal oscillations through calculation trajectories.

A remarkable effect of increasing the temperature was some water molecules split on the ZnO system at 600 K, forming Zn−OH groups on the surface after 8.7 ps of simulation. As an extrapolation to long-term simulation, this may affect the stability of the surface and become the seed for the dissolution of the surface, i.e., Zn−O−Zn bonds being broken in the slab to form $ZnO_{1-x}(OH)_{2x}$ species in solution[31]. In the case of TiO_2, no reactivity of water on the surface was observed. This may be related to the much lower solubility of TiO_2[45] with respect to ZnO due to the difficulty of starting the breaking of Ti−O bonds.

Finally, in both ZnO and TiO_2, there exists an increase in the distance between the metal atoms forming the first and last layers of the MO crystals, from 10.1 to 10.5 Å, for the ZnO slab, and from 18.9 to 20.7 Å for TiO_2, indicating a clear thermal expansion of the solid structure.

2.2.2. Analysis of the Interaction of the Hydrogenated MO Surface with Water at 300 K. We modified the O-terminated surface on the slabs to mimic low pH regimens in the system, limited to noncharged surfaces. An H atom was situated on top of each O atom of the corresponding surface (1 monolayer (ML) of H atoms) to saturate the surface with O−H bonds. In the case of ZnO, only the O-terminated surface was saturated with H; for TiO_2, the two symmetric surfaces were saturated with H. This model does not englobe all the features of a low pH medium; nevertheless, it is a first step to studying the interaction of water with hydrogenated MO surfaces.

For TiO_2, the saturated surfaces (with 8 H atoms per side) were stable during the whole MD simulation, and we could make an analogous analysis as in the previous sections. However, for ZnO, simulations led to a very different result. The formation of O−H bonds on the surface led to the instability of the internal ZnO bonds and the slab structure changed; this led to systems that chemically did not follow the same perfect crystal surface structure, and the systematic analysis performed in previous sections could not be extended in this case. Furthermore, to try to avoid the effects of disrupting the ZnO slab with the H saturation, we made tests decreasing the amount of H on the surface for 1, 0.5, 0.25 ML, ··· down to the minimum saturation of one single H atom on the O-terminated surface, corresponding to 0.125 ML. In all cases, the internal ZnO slab structure was affected by the presence of the O−H bonds of the surface, indicating a

https://doi.org/10.1021/acsomega.4c07557
ACS Omega 2025, 10, 4449−4457

potential initial step for the ZnO surface dissolution. It is noteworthy to mention that this difference in the chemistry of ZnO and TiO_2 surface with respect to H saturation may be related to the different solubility of both metal oxides, being the ZnO 3 orders of magnitude more soluble than TiO_2 and indicating an initialization of the dissolution mechanism.[46−48] This is again in agreement with the previous section, where reactivity on the ZnO surface was observed, whereas TiO_2 was inert with no reaction starting.

When analyzing MD simulations at 300 K changes of the hydrogenated structure in TiO_2 (Figures 1 and 2, insets (3,2)) with respect to bare TiO_2 (insets (1,2)) with water, unit cells were increased by 2 Å to accommodate the two extra H layers on the surface. Therefore, all peaks were displaced 1 Å to the sides with respect to the bare system. As a general trend, neither the bulk of water nor the inner slab peaks were affected by the presence of the H layer, and only the interface region showed changes referring to the bare surface.

In Figure 1 inset (3,2), peaks at −12.5 and 12.5 Å decreased in intensity and split into secondary small peaks at −12.25 and 12.25 Å. Also, the double peaks corresponding to the first solvation layer at −10.5 and −9.5 Å, and the corresponding at the other surface of the slab, got broader and less spiky, indicating that water-slab interaction was less effective when the TiO_2 surface got saturated with H; corroborated by the almost disappearing of the second solvation layer, which was present in the bare surface.

For the electronic structure analysis, Figure 2 (3,2) shows that peaks and lines corresponding to slab TiO_2, and bulk water, are barely affected by the H layer; nevertheless, one observes significant changes in the interface regions between −15 and −10 Å (and the symmetric correspondence at positive *x*-axis values). Ti atoms electrons (red line) in the first TiO layer of the surfaces (−13.5 and 13.5 Å, on both faces of the slab) decrease from 0.9 e^- on the bare surface down to 0.55 e^- to the most exposed ones. This is associated with the reduction of Ti^{4+} to Ti^{3+}, as observed in DFT calculations.[43] In the case of H (black line), the surface of the O−H layer is at −12.5 Å (and the corresponding at 12.5 Å). This layer affects water H atoms; for the bare surface, there was an accumulation of H charge at the surface (baseline in the bulk of 0.35 e^- converted into a peak of 0.4 e^-); nevertheless, for the hydrogenated surface this feature of accumulation is lost, and one observes two tiny peaks (a variation in the baseline of <0.1 e^-) at the interface of the H line corresponding to the O−H bond and the first water solvation layer on the slab. Finally, Oxygen electronic distribution shows in the bare surface (Figure 1(3,2)) an empty zone at −11.5 and 11.5 Å, due to the ordering and orientation of the waters on the first solvation layer; this feature is lost in the hydrogenated surface probably due to the weaker interaction between the hydrogenated surface and water molecules in the first solvation layer.

3. DISCUSSION

In this study, we performed SCC-DFTB/MD calculations in a systematic way to explore the electronic and structural dynamics of water and zinc oxide/titanium dioxide interfaces (as an example for a more general perspective for MO materials) under realistic conditions (temperature and density). Furthermore, as a result of our methodology, we provided information about the stability and convergence of simulation models under specific chemical conditions at the DFTB level, although longer simulation periods may be necessary to explore further chemical reactions on the surfaces.

The first group of models in this work represents MO surfaces in aqueous conditions at 300 K, with the TiO_2 slab being symmetric, whereas the ZnO is asymmetric. There exists a first solvation shell on the surface and a weaker second solvation layer. Distances of peaks representing the slab MO surface and the first water solvation shell agree with previous literature[37−39] for single and double water molecules adsorbed on the surfaces, as well as models with only one solvation layer at the DFT level. At 600 K, those second water layer peaks become flat, as expected from a higher kinetic energy regimen.

The second group of models deals with the interaction of MO surfaces with water at 600 K. Peaks corresponding to second solvation water shells vanish, whereas those for the first solvation layer are less intense. Charge distribution lines of metal atoms decrease as a general trend, associated with the larger atomic mobility in ZnO, the general profile of the charge peaks remains, whereas in the TiO_2 model, a significant decrease shows up on both surfaces, and this effect weakens from the MO surface toward the interior.

The last group of simulations was a first approximation to simulate low pH conditions, with a hydrogen layer on top of the MO surfaces; although the hydrogenated TiO_2 model converged under those conditions, the hydrogenated ZnO model was not stable. Due to the geometric and electronic calculation steps, which are not naturally possible (at initial steps of MD, hydrogenated structures showed negatively charged Zn atoms) that occur with the inclusion of hydrogen atoms in the system, results had to be excluded from the analysis. However, this may be a sign of an initialization mechanism for ZnO surface dissolution and the release of Zn ions to the medium.

For hydrogenated TiO_2 simulations, the direct surface interaction of water molecules was reduced by the H shielding with respect to the bare TiO_2 surface. In charge analysis, at −11.7 and 11.5 Å, peaks due to H new layer on the surface appears by hilling in the black line. As a consequence, the shielding of H atoms makes the TiO_2−water interaction less effective, and the charge transfer from the TiO_2 slab surface water molecules is less effective.

As a final remark, no reactivity causing surface modification was encountered in the models at room temperature, beyond the aforementioned case of the hydrogenated ZnO surface. On hydrogenated surfaces and high-temperature conditions, oxygen atoms on the surface could torsion, and on hydrogenated surfaces, the hydrogen atom layer was stable on the surface. The method used combining DFTB/MD offers a good capability to study the dynamics of MO-aqueous interfaces at room temperature conditions in combination with a lower computational cost than DFT.

4. METHODS

This work was performed in the framework of density functional tight binding (DFTB), a method based on the truncation of the Taylor expansion of the electronic structure calculations, which results in good agreement with ab initio density functional theory (DFT) calculations. In this manner, it is two to three orders of magnitude faster than DFT methods.[49,50] The method provides qualitatively correct results for the electronic and geometrical structures. Because of its advantages, the DFTB method is increasingly demanded, in exploring chemistry besides ab initio or DFT methods.[51−54]

https://doi.org/10.1021/acsomega.4c07557
ACS Omega 2025, 10, 4449−4457

Currently, the synergetic use of MD simulations and DFTB brings the possibility of describing dynamic systems as liquid water.[53,54] In a previous study,[8,9,35] DFT (on VASP)[55,56] and DFTB (on DFTB+)[51,57] methods showed consistent qualitative results and trends for anatase and rutile crystals, referring to the reliability and robustness of the less costly methods.[35]

4.1. Computational Details. In this work, DFTB+[51,57] software was employed to perform DFTB/MD simulations at the self-consistent charge (SCC)DFTB technique (also known as DTFB2).[58−60] Code version 20.1[61] of DFTB+ was executed.

The energy of the systems was evaluated in the first Brillouin zone on the Γ-point. System components are described with the atomic interaction using the Slater-Koster files from the Ti-org,[62] Zn-org,[63] and Mio[51] parameter sets. Those SK files do not include the correction for dispersion forces in the system because the dispersion parameters for Ti are not publicly available. Therefore, to maintain consistency in calculations, all parameters used in this work are at the DFTB2 level, including Zn, O, and H. All included simulation systems in this study were carried out in periodic boundary conditions (PBC).

Constant temperatures at 300 and 600 K were applied for simulations using the Nosé−Hoover chain thermostat algorithm[64] in the NVT ensemble. All MD simulations were carried out using the velocity−Verlet algorithm. All atoms were allowed to move freely due to kinetic energy coming from finite temperature MD.[65] Simulations were run from 10 (simulations for bare systems at 300 K) to 15 ps (simulations at 600 K or hydrogenated surfaces at 300 K) with 1.0 fs timesteps. To compute the time average properties, the first 2 ps of simulations were discarded as pre-equilibration time, as shown in Figure S2 in the Supporting Information. The total electronic energies converged through a maximum of 1000 SCC cycles or until a difference of 10^{-4} eV or lower in consecutive SCC cycles was found, ensuring the numerical stability. Electronic charges were calculated using the Mulliken population analysis implemented in the DFTB+ software. The Ewald summation procedures were automatically activated in DFTB+ to correct the existence of permanent dipoles in the system.

Finally, for the analysis of the obtained data, we built a script that plots a distribution figure for species' electronic charge and O atom accumulation per unit area. The analysis was based on the time-averaged analysis of all time steps in the perpendicular axis to the surface in a grid sectioned in the intervals of δz = 0.05 Å. In the final plot, two consecutive unit cells of periodic calculation were maintained, exposing solvent interactions between solid layers of MOs. In order to accelerate the analysis without losing information, only one trajectory every five steps was taken into account in the time-averaging process.

Finally, in order to compare electronic structure parameters, we computed time-averaged bandgap values from energetically equilibrated trajectory frames (Supporting Information, Section S3). DFTB shows for bulk ZnO wurzite and TiO_2 anatase[51,62,63] band gaps of 4.1 and 3.2 eV, closer to band gap experimental values (3.3 and 3.2 eV, respectively) than pure DFT GGA calculations (0.9 and 2.1 eV,[66] respectively). The simulation of band gaps in our solvated systems showed band gaps of ∼3.2−3.3 eV for ZnO-H_2O and ∼2.6−3.0 eV for TiO_2−H_2O, close to those of bulk materials. It is noteworthy that the hydrogenation of the TiO_2 surface makes the system a conductor and the band gap vanishes due to the presence of hydrogens on the surface.

4.2. Simulation Models. The ZnO (001) wurtzite surface slab model used in our calculations consisted of 128 atoms (64 Zn, 64 O), which was formed by a supercell with the lattice parameters of $a = b$ = 12.99 Å, ab = 60° angle, and c = 27.46 Å. The TiO_2 (101) Anatase surface slab model consisted of 288 atoms (96 Ti, 192 O), which was formed by a supercell with the lattice parameters of a = 15.08, b = 10.28, and c = 43.87 Å.

Due to the PBC calculations, slab models were naturally grouped in tiers. H_2O molecules were then included in the unit cell as liquid components of the system. Concurrently, 2.0 Å of the interaction zone between the added water boxes and water-facing solid surfaces was preserved for the initial MD steps. Allocated water boxes in unit cells have been framed in lattice vector sizes. Total water heights (on the Z-axis) were 15 and 20 Å for ZnO and TiO_2 setups, respectively.

The size of the supercell, the thickness of the water box, and the adjustment of lattice parameters were determined after conducting prior simulations on bulk material and water boxes that analyzed specific details such as density, average energy, and simulation temperature, as determined in previous work.[39,42]

To mimic natural system conditions, the water density was maintained at its natural density (ρ = 1 g·cm^{-3}) by including the proportional number of water molecules (73 and 112 H_2O molecules for ZnO and TiO_2, respectively). Figure 3 illustrates the studied models in their initial configurations.

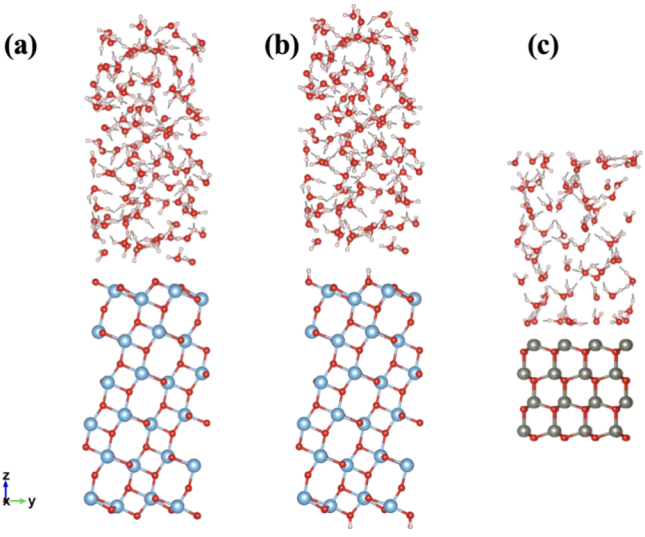

Figure 3. TiO_2 (a), hydrogenated TiO_2 (b) anatase, and ZnO (c) wurtzite models. Red is for oxygen, blue for titanium, gray for zinc and white for hydrogen.

Finally, we hydrogenated the terminal O atoms of the ZnO (001) and TiO_2 (101) surfaces to examine chemical modifications on the MO surface for simulations at 300 K. Hydrogen atoms were placed at 1 Å outward from the surface oxygens (16H for each MO). For TiO_2, hydrogen atoms were placed on both sides. For ZnO, hydrogenation occurred only for the O-terminated side of the ZnO (001) surface. Each Hydrogenated surface is reflected as an additional 1 Å to c dimension of the aforementioned unit cells. Further clarification regarding models, the data collection process

https://doi.org/10.1021/acsomega.4c07557
ACS Omega 2025, 10, 4449−4457

described in the reference data set,[67] and Supporting Information (Figure S3).

■ ASSOCIATED CONTENT

Data Availability Statement

The research data of this study is available at: https://doi.org/10.34810/DATA1411.

Supporting Information

The Supporting Information is available free of charge at https://pubs.acs.org/doi/10.1021/acsomega.4c07557.

Formal charges distributions on MO-water models; MD prestabilization analysis; time-averaged band gap values; time-averaged oxygen accumulation; and charge dynamics (PDF)

■ AUTHOR INFORMATION

Corresponding Author

Yarkın A. Çetin − *Departament d'Enginyeria Informàtica i Matemàtiques, Universitat Rovira i Virgili, 43007 Tarragona, Catalunya, Spain;* orcid.org/0000-0003-2456-5949; Email: yarkinaybars.cetin@urv.cat

Authors

Laura Escorihuela − *Departament d'Enginyeria Química, Universitat Rovira i Virgili, 43007 Tarragona, Catalunya, Spain;* orcid.org/0000-0002-6350-2396

Benjamí Martorell − *Escola de Doctorat, Universitat Rovira i Virgili, 43002 Tarragona, Catalunya, Spain; Departament d'Enginyeria Química, Universitat Rovira i Virgili, 43007 Tarragona, Catalunya, Spain;* orcid.org/0000-0002-7759-8042

Francesc Serratosa − *Departament d'Enginyeria Informàtica i Matemàtiques, Universitat Rovira i Virgili, 43007 Tarragona, Catalunya, Spain;* orcid.org/0000-0001-6112-5913

Complete contact information is available at: https://pubs.acs.org/10.1021/acsomega.4c07557

Author Contributions

Y.A.Ç. performed the calculations, wrote the paper, and analyzed the results; L.E. performed calculations and analyzed the results; B.M. analyzed the results and wrote the manuscript; F.S. designed the research project and wrote the paper.

Notes

The authors declare no competing financial interest.

■ ACKNOWLEDGMENTS

This project has received funding from the European Union's Horizon 2020 research and innovation programme under grant agreements NanoInformaTIX (H2020-NMBP-14-2018-814426) and Sbd4Nano (H2020-NMBP-TO-IND-2019-862195). Moreover, the AGAUR research group 2021SGR-00111: "ASCLEPIUS: Smart Technology for Smart Healthcare."

■ REFERENCES

(1) Kapinder, D. K.; Verma, A. K. Efficient & eco-friendly smart nano-pesticides: Emerging prospects for agriculture. *Mater. Today Proc.* **2021**, *45*, 3819−3824.

(2) Bhushan, I.; Singh, V. K.; Tripathi, D. K.editors. *Nanomaterials and Environmental Biotechnology*; Springer, 2020.

(3) Grzybowski, B. A.; Huck, W. T. S. The nanotechnology of life-inspired systems. *Nat. Nanotechnol.* **2016**, *11*, 585−592.

(4) Blaznik, U.; Krušič, S.; Hribar, M.; Kušar, A.; Žmitek, K.; Pravst, I. Use of Food Additive Titanium Dioxide (E171) Before the Introduction of Regulatory Restriction Due to Concern for Genotoxicity. *Foods* **2021**, *10*, 1910.

(5) Huh, A. J.; Kwon, Y. J. Nanoantibiotics": a new paradigm for treating infectious diseases using nanomaterials in the antibiotics resistant era. *J. Controlled Release* **2011**, *156*, 128−145.

(6) Zhu, M.; Nie, G.; Meng, H.; Xia, T.; Nel, A.; Zhao, Y. Physicochemical properties determine nanomaterial cellular uptake, transport, and fate. *Acc. Chem. Res.* **2013**, *46*, 622−631.

(7) Mancardi, G.; Mikolajczyk, A.; Annapoorani, V. K.; Bahl, A.; Blekos, K.; Burk, J., et al. A computational view on nanomaterial intrinsic and extrinsic features for nanosafety and sustainability. *Mater. Today* **2023**. *67*344.

(8) Çetin, Y. A.; Martorell, B.; Serratosa, F. Prediction of electronic density of states in guanine-TiO2 adsorption model based on machine learning. *Computational and Structural Biotechnology Reports* **2024**, *1*, No. 100008.

(9) Çetin, Y. A.; Martorell, B.; Serratosa, F.; Calatayud, M. Adsorption of Guanine on Oxygen-Deficient TiO2 Surface: A Combined MD-DFTB/DFT Strategy. *ACS Omega* **2024**. 939043.

(10) Haider, A. J.; Jameel, Z. N.; Al-Hussaini, I. H. M. Review on: Titanium Dioxide Applications. *Energy Procedia* **2019**, *157*, 17−29.

(11) Chen, X.; Selloni, A. Introduction: Titanium Dioxide (TiO2) Nanomaterials. *Chem. Rev.* **2014**, *114*, 9281−9282.

(12) Tan, M. H.; Commens, C. A.; Burnett, L.; Snitch, P. J. A pilot study on the percutaneous absorption of microfine titanium dioxide from sunscreens. *Australasian Journal of Dermatology* **1996**, *37*, 185−187.

(13) Moran, C. A.; Mullick, F. G.; Ishak, K. G.; Johnson, F. B.; Hummer, W. B. Identification of titanium in human tissues: Probable role in pathologic processes. *Hum Pathol* **1991**, *22*, 450−454.

(14) Brayner, R. The toxicological impact of nanoparticles. *Nano Today* **2008**, *3*, 48−55.

(15) Cho, W. S.; Duffin, R.; Bradley, M.; Megson, I. L.; MacNee, W.; Lee, J. K.; et al. Predictive value of in vitro assays depends on the mechanism of toxicity of metal oxide nanoparticles. *Part Fibre Toxicol* **2013**, *10*, 10.

(16) Palomäki, J.; Karisola, P.; Pylkkänen, L.; Savolainen, K.; Alenius, H. Engineered nanomaterials cause cytotoxicity and activation on mouse antigen presenting cells. *Toxicology* **2010**, *267*, 125−131.

(17) Watson, C.; Ge, J.; Cohen, J.; Pyrgiotakis, G.; Engelward, B. P.; Demokritou, P. High-throughput screening platform for engineered nanoparticle-mediated genotoxicity using cometchip technology. *ACS Nano* **2014**, *8*, 2118−2133.

(18) Kim, I. S.; Baek, M.; Choi, S. J. Comparative cytotoxicity of Al2O3, CeO2, TiO2 and ZnO nanoparticles to human lung cells. *J. Nanosci Nanotechnol* **2010**, *10*, 3453−3458.

(19) Pathakoti, K.; Morrow, S.; Han, C.; Pelaez, M.; He, X.; Dionysiou, D. D.; et al. Photoinactivation of Escherichia coli by sulfur-doped and nitrogen-fluorine-codoped TiO2 nanoparticles under solar simulated light and visible light irradiation. *Environ. Sci. Technol.* **2013**, *47*, 9988−9996.

(20) Shukla, R. K.; Sharma, V.; Pandey, A. K.; Singh, S.; Sultana, S.; Dhawan, A. ROS-mediated genotoxicity induced by titanium dioxide nanoparticles in human epidermal cells. *Toxicol In Vitro* **2011**, *25*, 231−241.

(21) Li, Y.; Niu, J.; Zhang, W.; Zhang, L.; Shang, E. Influence of aqueous media on the ROS-mediated toxicity of ZnO nanoparticles toward green fluorescent protein-expressing Escherichia coli under UV-365 irradiation. *Langmuir* **2014**, *30*, 2852−2862.

(22) Appierot, G.; Lipovsky, A.; Dror, R.; Perkas, N.; Nitzan, Y.; Lubart, R. Enhanced Antibacterial Activity of Nanocrystalline ZnO Due to Increased ROS-Mediated Cell Injury. *Adv. Funct. Mater.* **2009**, *19*, 842−852.

(23) Li, Y.; Zhang, W.; Niu, J.; Chen, Y. Mechanism of photogenerated reactive oxygen species and correlation with the antibacterial properties of engineered metal-oxide nanoparticles. *ACS Nano* **2012**, *6*, 5164−5173.
(24) Kumar, A.; Pandey, A. K.; Singh, S. S.; Shanker, R.; Dhawan, A. Engineered ZnO and TiO(2) nanoparticles induce oxidative stress and DNA damage leading to reduced viability of Escherichia coli. *Free Radic Biol. Med.* **2011**, *51*, 1872−1881.
(25) Djurišić, A. B.; Leung, Y. H.; Ng, A. M. C.; Xu, X. Y.; Lee, P. K. H.; Degger, N.; et al. Toxicity of metal oxide nanoparticles: mechanisms, characterization, and avoiding experimental artefacts. *Small* **2015**, *11*, 26−44.
(26) Aruguete, D. M.; Hochella, M. F.; Aruguete, D. M.; Hochella, M. F. Bacteria−nanoparticle interactions and their environmental implications. *Environ. Chem.* **2010**, *7*, 3−9.
(27) von Moos, N.; Slaveykova, V. I. Oxidative stress induced by inorganic nanoparticles in bacteria and aquatic microalgae–state of the art and knowledge gaps. *Nanotoxicology* **2014**, *8*, 605−630.
(28) Liu, J.; Feng, X.; Wei, L.; Chen, L.; Song, B.; Shao, L. The toxicology of ion-shedding zinc oxide nanoparticles. *Crit Rev. Toxicol* **2016**, *46*, 348−384.
(29) Ho, M.; Wu, K. Y.; Chein, H. M.; Chen, L. C.; Cheng, T. J. Pulmonary toxicity of inhaled nanoscale and fine zinc oxide particles: mass and surface area as an exposure metric. *Inhal Toxicol* **2011**, *23*, 947−956.
(30) Rousseau, R.; Glezakou, V. A.; Selloni, A. Theoretical insights into the surface physics and chemistry of redox-active oxides. *Nature Reviews Materials* **2020**, *5*, 460−475.
(31) Singh, S.; Prasad, S. M.; Bashri, G. Fate and toxicity of nanoparticles in aquatic systems. *Acta Geochimica* **2023**, *42*, 63−76.
(32) Saxena, P.; Harish, S. D.; Vats, K.; Miglani, R.; Singh, A. K. A critical review on fate, behavior, and ecotoxicological impact of zinc oxide nanoparticles on algae. *Environ. Sci. Pollut. Res.* **2024**, *31*, 19105−19122.
(33) Zheng, T.; Wu, C.; Chen, M.; Zhang, Y.; Cummings, P. T. A DFT study of water adsorption on rutile TiO2 (110) surface: The effects of surface steps. *J. Chem. Phys.* **2016**, *145*, 44702.
(34) Li, J. Q.; Sun, Y.; Cheng, J. Theoretical investigation on water adsorption conformations at aqueous anatase TiO2/water interfaces. *J. Mater. Chem. A Mater.* **2023**, *11*, 943−952.
(35) Çetin, Y. A.; Martorell, B.; Serratosa, F.; Aguilera-Porta, N.; Calatayud, M. Analyzing the TiO2 surface reactivity based on oxygen vacancies computed by DFT and DFTB methods. *J. Phys.: Condens. Matter* **2022**. *34*314004.
(36) Li, W.; Kotsis, K.; Manzhos, S. Comparative density functional theory and density functional tight binding study of arginine and arginine-rich cell penetrating peptide TAT adsorption on anatase TiO2. *Phys. Chem. Chem. Phys.* **2016**, *18*, 19902−19917.
(37) Kenmoe, S.; Ulrich, B. P. Water aggregation and dissociation on the ZnO(1010) surface. *Phys. Chem. Chem. Phys.* **2017**, *19*, 1466−1486.
(38) Cong, V. T.; Van Son, N.; Diem, D. Q.; Pham, S. Q. T. A comparison of water−gas shift reaction on ZnO (10 $\bar{1}$ 0) surface and 6Cu cluster deposited over ZnO (10 $\bar{1}$ 0) surface using density functional theory studies. *J. Mol. Model* **2022**, *28*, 1−11.
(39) große Holthaus, S. *Molecular Dynamics Simulations of ZnO: A step by step approach towards a detailed understanding of the complex solid/liquid/bio interface*. Universität: Bremen (Germany), 2014.
(40) Bandura, A. V.; Kubicki, J. D. Derivation of force field parameters for TiO2-H2O systems from ab initio calculations. *J. Phys. Chem. B* **2003**, *107*, 11072−11081.
(41) Allegretti, F.; O'Brien, S.; Polcik, M.; Sayago, D. I.; Woodruff, D. P. Adsorption bond length for H2O on TiO2(110): A key parameter for theoretical understanding. *Phys. Rev. Lett.* **2005**, *95*, No. 226104.
(42) Jin, M.; Yan, S.; Chen, D. Adsorption mechanism of water molecules on the surface of ZnO-SAW sensors. *Chem. Phys.* **2020**, *538*, No. 110915.
(43) Gutiérrez Moreno, J. J.; Fronzi, M.; Lovera, P.; O'Riordan, A.; Ford, M. J.; Li, W.; et al. Structure, stability and water adsorption on ultra-thin TiO2 supported on TiN. *Phys. Chem. Chem. Phys.* **2019**, *21*, 25344−25361.
(44) Orozco, I.; Huang, E.; Gutiérrez, R. A.; Liu, Z.; Zhang, F.; Mahapatra, M.; et al. Hydroxylation of ZnO/Cu(1 1 1) inverse catalysts under ambient water vapor and the water-gas shift reaction. *Journal of Physics D* **2019**, *52*, 454001.
(45) Oskam, G.; Poot, D. J. P. Synthesis of ZnO and TiO2 nanoparticles. *J. Solgel Sci. Technol.* **2006**, *37*, 157−160.
(46) Reed, R. B.; Ladner, D. A.; Higgins, C. P.; Westerhoff, P.; Ranville, J. F. Solubility of nano-zinc oxide in environmentally and biologically important matrices. *Environ. Toxicol. Chem.* **2012**, *31*, 93−99.
(47) Franklin, N. M.; Rogers, N. J.; Apte, S. C.; Batley, G. E.; Gadd, G. E.; Casey, P. S. Comparative toxicity of nanoparticulate ZnO, bulk ZnO, and ZnCl2 to a freshwater microalga (Pseudokirchneriella subcapitata): The importance of particle solubility. *Environ. Sci. Technol.* **2007**, *41*, 8484−8490.
(48) Avramescu, M. L.; Rasmussen, P. E.; Chénier, M.; Gardner, H. D. Influence of pH, particle size and crystal form on dissolution behaviour of engineered nanomaterials. *Environ. Sci. Pollut Res. Int.* **2017**, *24*, 1553−1564.
(49) Selli, D.; Fazio, G.; di Valentin, C. Using Density Functional Theory to Model Realistic TiO2 Nanoparticles, Their Photoactivation and Interaction with Water. *Catalysts* **2017**, *7*, 357.
(50) Selli, D.; Fazio, G.; Seifert, G.; Di Valentin, C. Water Multilayers on TiO2 (101) Anatase Surface: Assessment of a DFTB-Based Method. *J. Chem. Theory Comput* **2017**, *13*, 3862−3873.
(51) Elstner, M.; Porezag, D.; Jungnickel, G.; Elsner, J.; Haugk, M.; Frauenheim, T. Self-consistent-charge density-functional tight-binding method for simulations of complex materials properties. *Phys. Rev. B* **1998**, *58*, 7260.
(52) Gruden, M.; Andjelkovic, L.; Jissy, A. K.; Stepanović, S.; Zlatar, M.; Cui, Q.; et al. Benchmarking density functional tight binding models for barrier heights and reaction energetics of organic molecules. *J. Comput. Chem.* **2017**, *38*, 2171−2185.
(53) Kaminski, S.; Gaus, M.; Elstner, M. Improved electronic properties from third-order SCC-DFTB with cost efficient post-SCF extensions. *J. Phys. Chem. A* **2012**, *116*, 11927−11937.
(54) Galvão, B. R. L.; Viegas, L. P.; Salahub, D. R.; Lourenço, M. P. Reliability of semiempirical and DFTB methods for the global optimization of the structures of nanoclusters. *J. Mol. Model* **2020**, *26*, 1−8.
(55) Kresse, G.; Furthmüller, J. Efficiency of ab-initio total energy calculations for metals and semiconductors using a plane-wave basis set. *Comput. Mater. Sci.* **1996**, *6*, 15−50.
(56) Kresse, G.; Furthmüller, J. Efficient iterative schemes for ab initio total-energy calculations using a plane-wave basis set. *Phys. Rev. B* **1996**, *54*, 11169.
(57) Aradi, B.; Hourahine, B.; Frauenheim, T. DFTB+, a Sparse Matrix-Based Implementation of the DFTB Method†. *J. Phys. Chem. A* **2007**, *111*, 5678−5684.
(58) Seifert, G. Tight-Binding Density Functional Theory: An Approximate Kohn−Sham DFT Scheme†. *J. Phys. Chem. A* **2007**, *111*, 5609−5613.
(59) Koskinen, P.; Mäkinen, V. Density-functional tight-binding for beginners. *Comput. Mater. Sci.* **2009**, *47*, 237−253.
(60) Porezag, D.; Frauenheim, T.; Köhler, T.; Seifert, G.; Kaschner, R. Construction of tight-binding-like potentials on the basis of density-functional theory: Application to carbon. *Phys. Rev. B* **1995**, *51*, 12947.
(61) Hourahine, B.; Aradi, B.; Blum, V.; Bonafé, F.; Buccheri, A.; Camacho, C.; et al. DFTB+, a software package for efficient approximate density functional theory based atomistic simulations. *J. Chem. Phys.* **2020**, *152*, 124101.
(62) Dolgonos, G.; Aradi, B.; Moreira, N. H.; Frauenheim, T. An Improved Self-Consistent-Charge Density-Functional Tight-Binding (SCC-DFTB) Set of Parameters for Simulation of Bulk and Molecular

https://doi.org/10.1021/acsomega.4c07557
ACS Omega 2025, 10, 4449−4457

Systems Involving Titanium. *J. Chem. Theory Comput* **2010**, *6*, 266−278.
(63) Moreira, N. H.; Dolgonos, G.; Aradi, B.; Da Rosa, A. L.; Frauenheim, T. Toward an Accurate Density-Functional Tight-Binding Description of Zinc-Containing Compounds. *J. Chem. Theory Comput* **2009**, *5*, 605−614.
(64) Martyna, G. J.; Tuckerman, M. E.; Tobias, D. J.; Klein, M. L. Explicit reversible integrators for extended systems dynamics. *Mol. Phys.* **1996**, *87*, 1117−1157.
(65) Hofer, T. S.; Tirler, A. O. Combining 2d-Periodic Quantum Chemistry with Molecular Force Fields: A Novel QM/MM Procedure for the Treatment of Solid-State Surfaces and Interfaces. *J. Chem. Theory Comput* **2015**, *11*, 5873−5887.
(66) Kovačič, Ž; Likozar, B.; Huš, M. Ab initio modelling of photocatalytic CO2 reduction reactions over Cu/TiO2 semi-conductors including the electronic excitation effects. *Chemical Engineering Journal* **2024**, *485*, No. 149894.
(67) Çetin, Y. A.; Escorihuela, L.; Martorell Masip, B.; Serratosa, F. *Replication Data for: Revisiting Water Adsorption on TiO2 and ZnO Surfaces: A SCC-DFTB Molecular Dynamics Study*; CORA, 2024, https://doi.org/10.34810/DATA1411.

https://doi.org/10.1021/acsomega.4c07557
ACS Omega 2025, 10, 4449−4457